An Automated Variable E-Field DFT Application (A.V.E.D.A.) for Evaluation of Optimally Oriented Electric Fields on Chemical Reactivity

Dalton J. Hanaway and C. Rose Kennedy*

Department of Chemistry, University of Rochester, Rochester, NY 14627, USA

E-mail: c.r.kennedy@rochester.edu

Abstract

Recent theoretical and experimental work at molecular junctions has provided a strong conceptualization for the effects of oriented electric fields (OEFs) on organic reactions. Depending upon the axis of application, OEFs can increase (or decrease) reaction rate or distinguish between enantiomeric pathways. Despite the conceptual elegance of OEFs, which may be applied externally or induced locally, as tools for catalyzing organic reactions, implementation in synthetically relevant systems has been hampered by inefficiencies in evaluating reaction sensitivity to field effects. Herein we describe the development of the Automated Variable Electric-Field DFT Application (A.V.E.D.A.) for streamlined evaluation of a reaction's susceptibility to OEFs. This open-source software was designed to be accessible for novice users of computational or programming tools. Following initiation by a single command (and with no subsequent intervention) the Linux workflow manages a series of density functional theory (DFT) calculations and mathematical manipulations to optimize ground-state

and transition-state geometries in oriented, electric fields of increasing magnitude. The resulting field-perturbed geometries, molecular and reaction dipole moments, and net effective activation energies are compiled for user interpretation. Ten representative pericyclic reactions that showcase the development and evaluation of A.V.E.D.A. are described.

Introduction

Achieving precise control over reactivity and selectivity is a defining goal of synthetic chemistry. Traditionally, this has been achieved through substrate, reagent, or catalyst control under carefully tuned reaction conditions including (for example) solvent, concentration, temperature, and time. By contrast, external electromagnetic stimuli have traditionally been relegated to spectroscopic characterization with little consideration for potential effects on chemical transformations more broadly. In a disruption to these traditional approaches, oriented electric fields (OEFs) have been identified as an alternative synthetic tool.[1–3] An applied electric field hyper-polarizes co-axial bonds, which in turn alters the effective barriers for transformations involving redistribution of electron density associated with changes in their bonding.[4] This phenomenon—called the electric field effect—has long been invoked as determining the catalytic efficiency of enzymes,[5–10] and spectroscopic work has quantified the field-induced component of enzymatic rate acceleration.[6,11,12]

Theoretical studies, most commonly examining a class of concerted [4+2]-cycloadditions (the Diels–Alder reaction), support the viability of OEFs as unconventional "catalysts" for synthetically relevant transformations (Figure 1A).[13,14] These studies further highlight sensitivity of OEF effects to alignment with the reaction axis, which is defined as the change in electron localization between ground and transition states.[12] In agreement with computational predictions, single molecule experiments examining Diels–Alder substrates immobilized at molecular junctions supported that C–C bond formation was accelerated or inhibited depending upon the orientation of the applied electric field (Figure 1B).[15]

These proof-of-principle results have inspired a burgeoning area of research that seeks to harness OEFs in synthetically practical systems through design of molecular capacitors,[16,17] electrostatically biased molecular frameworks, or intrinsic field-modified reagents.[3,18] Significant related work in inorganic and coordination chemistry has employed secondary coordination sphere electrostatic effects to alter redox potentials (ground-state effects).[19,20] This approach suggests using reagent or catalyst design to introduce local electric fields that modulate reactivity in bulk solution. However, harnessing field effects for synthetically useful reactivity is hampered by the tedious and technically arduous computational process of evaluating both the viability (magnitude of the possible electric field effect) and optimal orientation of the applied field.

Herein, a user-friendly application is presented to facilitate density functional theory calculations of chemical reactions in the presence of optimally oriented electric fields. The Automated Variable Electric Field DFT Application (A.V.E.D.A.) provides the first fully automated, electric field probe with DFT-level rigor. This approach is complementary to the Taylor-series expansion methodology developed by Luis and Torrent-Sucarrat,[21] which offers the trade-off between reduced precision and expedited computational efficiency when compared to DFT approaches (Figure 1C). Because each calculation with A.V.E.D.A. requires only a single command, with simple user specifications requiring minimal computational experience, this program is well-suited as a pre-screening tool for experimental electric field applications. Building from the marked OEF effects observed for Diels Alder reactions, the development and application of A.V.E.D.A. is described with a suite of mechanistically distinct pericyclic reactions as model transformations (Figure 1D). These test cases were selected due to their plausible synthetic utility and concerted (single-step) nature. Despite their limited sensitivity to traditional forms of catalysis, predictions obtained with A.V.E.D.A. support the broad viability of synthetically significant electric field effects across these families of pericyclic processes.

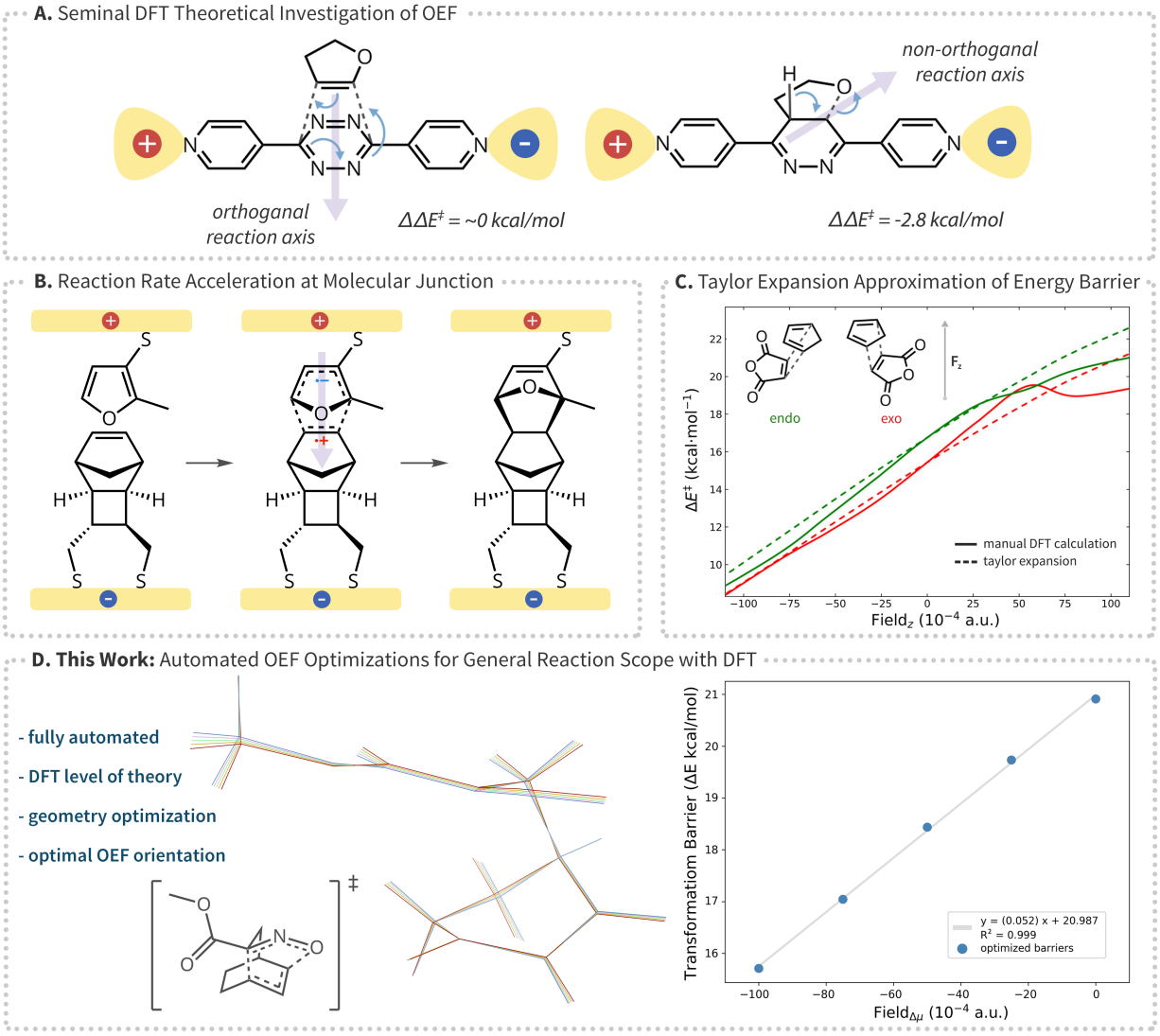

Figure 1: Methods for evaluating oriented electric field effects of chemical reactivity. Plot 1C reproduced with permission.[21] ©2021 The Authors. Published by American Chemical Society

Results and Discussion

A.V.E.D.A. Workflow Development

A.V.E.D.A. input consists of two *.xyz* files listing the unoptimized coordinates for ground-state and transition-state structures (guesses) for the transformation of interest. Output consists of optimized structures and energies at four increasingly strong electric field strengths.

To develop A.V.E.D.A.'s workflow and evaluate OEF results, pericyclic reactions were identified as an attractive transformation class. While the small system size enabled quick computation times and efficient algorithm development, the high activation energies posed synthetic challenge and thus motivated the possibility for improvements. Promising results obtained for the Diels–Alder reaction in an OEF suggested viability of OEF barrier reductions for a super-set of pericyclic reactions. Ten transformations—Cope elimination, Cope rearrangement, Claisen rearrangement, ene reaction, electrocyclic ring-opening/closing, and sigmatropic rearrangements ([1,5], [3,3], and [2,3])—were selected as the development data set (see Supporting Information for details). Two representative transformations are depicted in the main text to illustrate the capabilities and results obtained with A.V.E.D.A. (Figure 2).

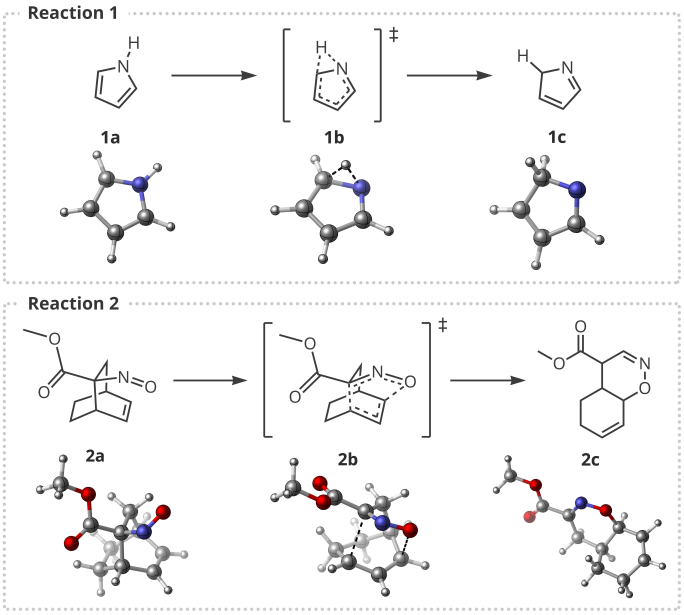

Figure 2: Representative pericyclic reactions used to develop A.V.E.D.A. and illustrate findings.

After instantiation of A.V.E.D.A. (see Computational Methods Section for details) all subsequent OEF calculations proceed automatically with no user intervention required (Figure 3). To begin each run, a new directory containing copies of all necessary A.V.E.D.A. scripts is created. Ground-state and transition-state structures are formatted into Gaussian

input files for initial optimization in the absence of an applied electric field and submitted to Slurm for computation.[22] Note that the Slurm workload manager is the standard scheduling tool for computing clusters. Next, corresponding atoms in the optimized transition states and intermediates are aligned in the Cartesian coordinate system using PyMol via a root-mean-square deviation (RMSD) distance reduction.[23]

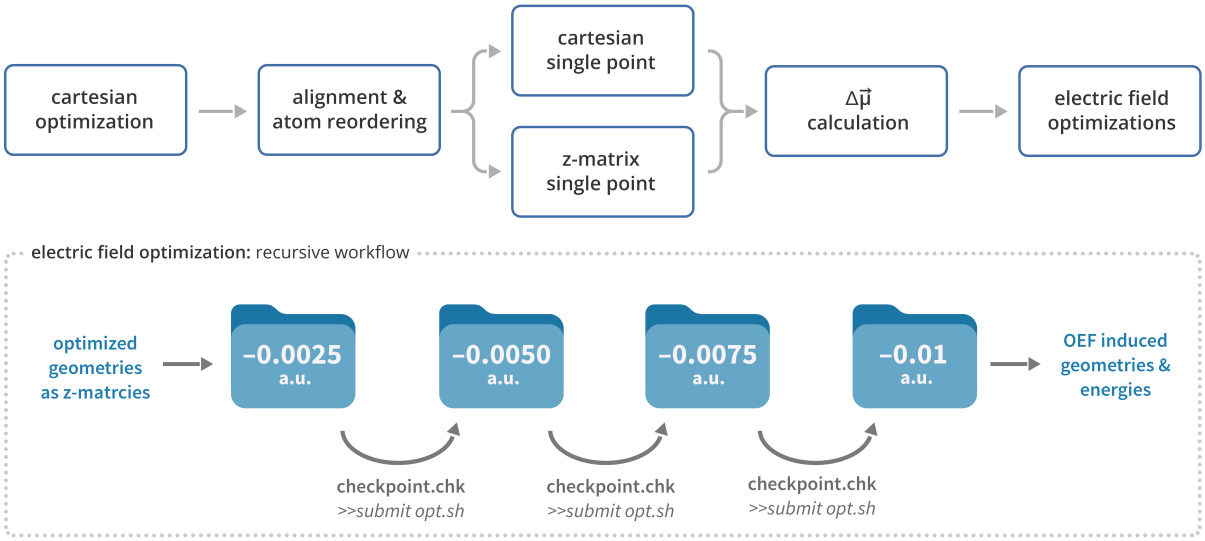

Figure 3: Overview of processes during an A.V.E.D.A. instance.

Atomic Coordinate Reordering. Subsequent calculation in an applied electric field utilizing the *Field* keyword must be performed on structures in the Z-matrix format. In contrast to the Cartesian format, the Z-matrix limits degrees of freedom by constraining *atom 1* at the origin, *atom 2* on the z-axis, *atom 3* on the x-axis, and *atom 4* on the y-axis. This constraint is necessary to prevent reorientation during the OEF optimization, and these four atoms are referred to as the "orientation atoms" throughout this work.

During development, it became clear that the input order of atomic coordinates (and therefore the quality of the Z-matrix) influenced the success of subsequent OEF optimization steps. To support successful implementation, the atomic coordinates for aligned structures were thus reordered by one of three methods, described below.

- *Method 0* preserves the original input ordering impacted only by Z-matrix construction

by the *newzmat* utility .

- *Method 1* was developed to maximize the stability of the orientation atoms in an electric field by calculating the unweighted Cartesian center of the transition state and moving the nearest three atoms to the orientation atom position. It is predicted these core atoms will have the least freedom for low energy free rotation during optimization.

- *Method 2* reorders atoms to minimize the geometry changes' influence on dipole-field orientation by choosing the atom furthest from the site of transformation. Rather than moving individual atoms, this remote atom and all subsequent atoms are moved in a block to the top of the input file so that connectivity represented by atom order is preserved to the greatest extent feasible.

During testing on the pericyclic data set it was determined that *method 1* was most suitable when fringe atoms could easily rotate (ex. a methyl group) or when the transition state was comprised of two unconnected fragments associated only by bond-breaking and forming (see Supporting Information for details). *Method 2* proved useful when *method 1* produced a low quality Z-matrix due to inconsistencies between atom order and molecular connectivity.

Dipole Moment Vector Algebra. Following alignment and reordering, single point calculations are performed in the Cartesian and Z-matrix input formats for both ground-state and transition-state structures. From these results, A.V.E.D.A. calculates the optimal electric field alignment given the transition state and intermediate dipole moments. First, the $\Delta\vec{\mu}$ dipole difference vector is calculated and normalized with eq. 1 as illustrated in Figure 4.

$$\Delta\vec{\mu} = \frac{\vec{ts}_{cart} - \vec{int}_{cart}}{\|\vec{ts}_{cart} - \vec{int}_{cart}\|} \tag{1}$$

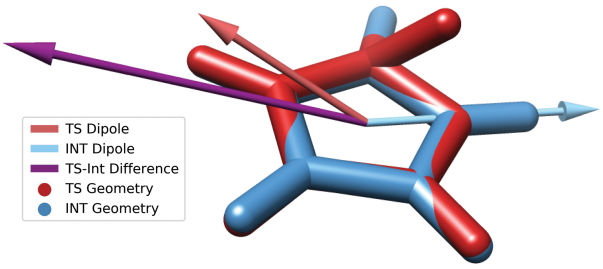

Figure 4: Example vector algebra shown for **1** to find the transition state (red) minus preceding ground state (blue) dipole difference direction (purple). The electric field is applied along the negative direction of this vector.

However, the ground-state and transition-state structures change orientation independently when when converted from the Cartesian to Z-matrix coordinate system for electric field optimizations. Therefore, the $\Delta\vec{\mu}$ direction must be mapped between the two orientations. This process is accomplished by generating a rotation matrix for the transition state and intermediate dipole moment from Cartesian to Z-matrix coordinates (eq. 2-4). The Cartesian $\Delta\vec{\mu}$ vector is translated with the rotation matrix, shown in eq. 4 for both structures into the Z-matrix coordinate system. The resulting normalized $\Delta\vec{\mu}_{int,z-mat}$ and $\Delta\vec{\mu}_{ts,z-mat}$ are then used as the directions along which OEFs are applied.

$$\mathbf{v} = \vec{\boldsymbol{\mu}}_{cart} \times \vec{\boldsymbol{\mu}}_{zmat} \tag{2}$$

$$\mathbf{v}_{\times} = \begin{bmatrix} 0 & -v_3 & v_2 \\ v_3 & 0 & -v_1 \\ -v_2 & v_2 & 0 \end{bmatrix} \tag{3}$$

$$\mathbf{R}_{cart\rightarrow zmat} = \mathbf{I}_3 + \mathbf{v}_{\times} + (\mathbf{v}_{\times} \cdot \mathbf{v}_{\times}) \left(\frac{1 - (\vec{\boldsymbol{\mu}}_{cart} \cdot \vec{\boldsymbol{\mu}}_{zmat})}{\|\mathbf{v}\|^2} \right) \tag{4}$$

Electric Field Application and Results Generation. Gaussian OEF optimization submission scripts are constructed with fields generated from scaling the $\Delta\vec{\mu}_{zmat}$ vectors by $(-25, -50, -75, and\ -100) \cdot 10^{-4}\ a.u.$. While the $-25 \cdot 10^{-4}$ starting point geometry is

read from the single point Z-matrix input file, all subsequent optimizations at stronger field strengths are recursively called on the previous checkpoint geometry once optimizations in the weaker field converges. After all eight OEF optimizations have converged, the output files are moved to the Results directory and analyzed.

OEF Results

For all ten pericyclic reactions in the development data set, A.V.E.D.A. produced results resembling those illustrated in Figure 5 for Reaction **2**. However, the success rate varied with respect to the atomic ordering method selected. A successful run was characterized by linear reductions in activation energy as a function of OEF magnitude—indicated by an R^2 greater than 0.95 and no discontinuous jumps in energy or molecular geometry—with appropriate imaginary vibrational frequencies for intermediates (0) and transition states (1). Atom ordering *method* 1 yielded a 80% success rate while *method* 0 and 2 were successful for 70% of the data set. Because each method was suitable for different types of geometries, overall the three methods covered 100% of the pericyclic reactions tested (see Supporting Information for details).

As shown in Figure 5, for all successful executions, A.V.E.D.A. generates a plot of activation energy (kcal/mol) as a function of OEF magnitude (a.u.) from the raw tabulated energy values. Additionally, a table is compiled of the ground-state and transition-state energies, and $\Delta\vec{\mu}$ molecular dipole results from optimized geometries aligned in the Cartesian coordinate system.

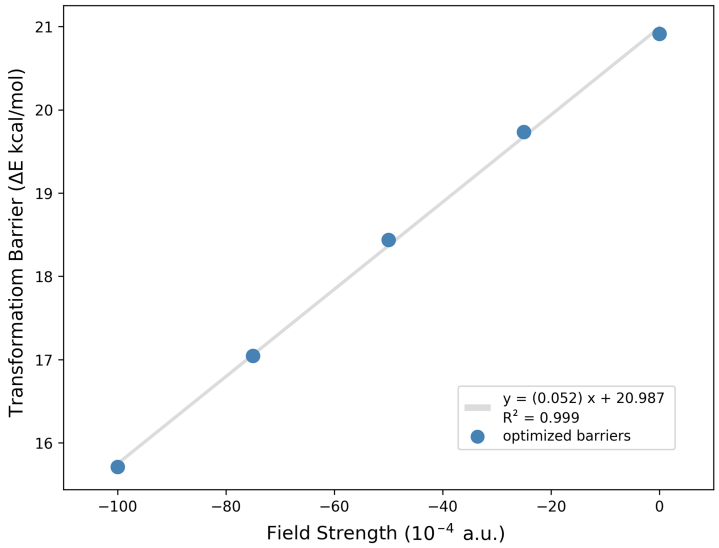

ts dipole moment (xyz)
[1.578, -2.851, 1.399]
||ts dipole|| = 3.546

gs dipole moment (xyz)
[0.064, -1.864, 1.618]
||int dipole|| = 2.469

ts-gs dipole moment (xyz)
[1.513, -0.987, -0.218]
||dipole difference|| = 1.820

results summary					
field strength (10^{-4} a.u.)	0	-25	-50	-75	-100
gs energy (a.u.)	-669.4711	-669.4724	-669.4747	-669.4780	-669.4826
ts energy (a.u.)	-669.4378	-669.4410	-669.4453	-669.4509	-669.4576
barrier ΔE (kcal/mol)	20.91	19.73	18.44	17.04	15.71
ΔΔE (kcal/mol)	0.00	-1.18	-2.48	-3.87	-5.20

Figure 5: Summary of A.V.E.D.A. output data for reaction **2**. Dipole moments for aligned intermediate and transition state geometry are shown in the top right while transformation barrier reductions ($\Delta\Delta$E) at each OEF strength are below.

Aligned Dipole Different Vector. Once a suitable program workflow had been developed and tested, A.V.E.D.A.'s results were validated by considering the electric field orientation with respect to $\Delta\vec{\mu}$ for reaction **1**. The A.V.E.D.A. algorithm was modified to apply an electric field along 18 vectors distributed over a unit sphere, in addition to the $\pm\Delta\vec{\mu}$ directions, each with a magnitude of $50 \cdot 10^{-4}$ $a.u.$. The field effects on the activation energy were normalized relative the unperturbed, yielding $\Delta\Delta E$, and multiplied by the unit vector along which the respective OEF was applied. Scaled vectors were plotted and colored by the positive (blue) or negative (red) $\Delta\Delta E$ calculated (Figure 6). The lowest activation energy—corresponding to the longest dark blue vector—was realized along $-\Delta\vec{\mu}$ while fields which increased the transformation barrier were found in the opposite direction (along $+\Delta\vec{\mu}$). Note

that the Gaussian 09 positive field direction is opposite to physics convention; thus applying an electric field along $-\Delta\vec{\mu}$ represents alignment between the field and reaction axis of the given transformation and stabilization of the dipole moment.[13] These data validate the assumption that the optimally oriented fields projects along $\Delta\vec{\mu}$ (used in the program workflow used to calculate this aligned $\Delta\vec{\mu}$ vector).

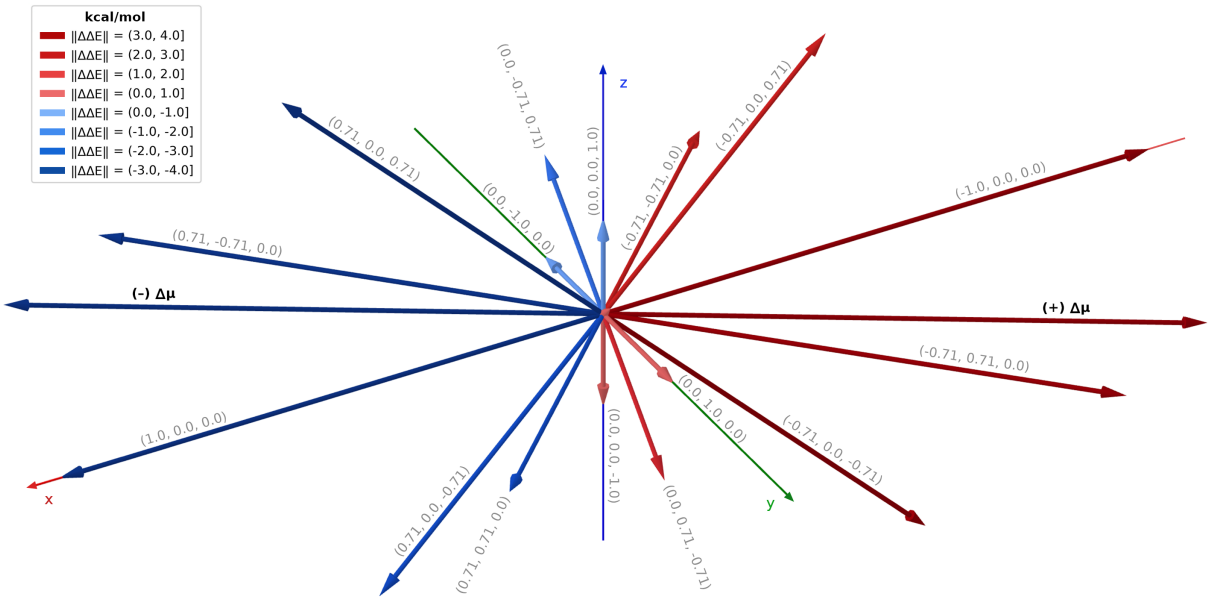

Figure 6: Vector's magnitude and color shade represent activation energy changes in $kcal/mol$ with a $5 \cdot 10^{-5}\, a.u.$ OEF applied along vector's direction (gray coordinates). Darker blue vectors indicate a reduction in activation energy while darker red show an increase.

OEF Effects on Transition State Geometry. The effects of applied OEFs on molecular geometry were investigated by overlaying aligned structures optimized at each field strength for a single transformation. A correlation between transition state geometry and OEF magnitude was observed for bonds involved in the transformation of interest (Figure 7). In the presence of increasingly strong OEFs, the transition-state geometry tended towards ground-state bond lengths and thus an earlier transition state. While the breaking C–C bond elongates slightly by 0.05 Å the forming C–O bond grows by 0.274 Å yielding a net 0.224 Å shift towards the intermediate lengths (see Supporting Information for details). The reaction coordinate in Figure 8 illustrates this result for Reaction **2**.

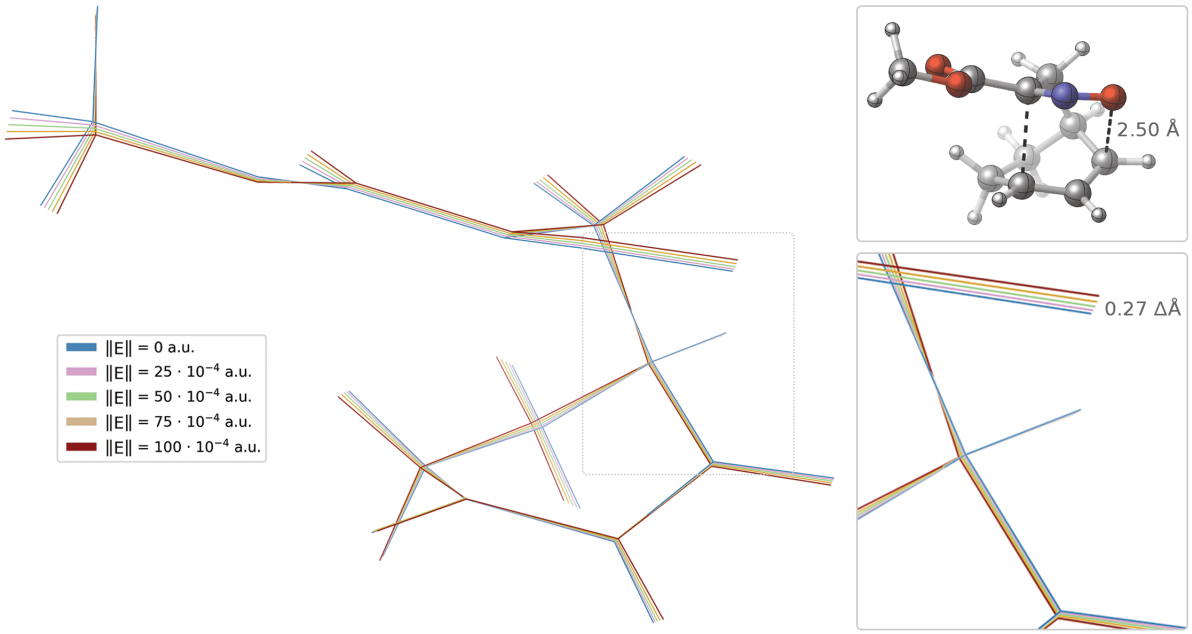

Figure 7: Comparison of transition state geometry **2b** with respect to the OEF.

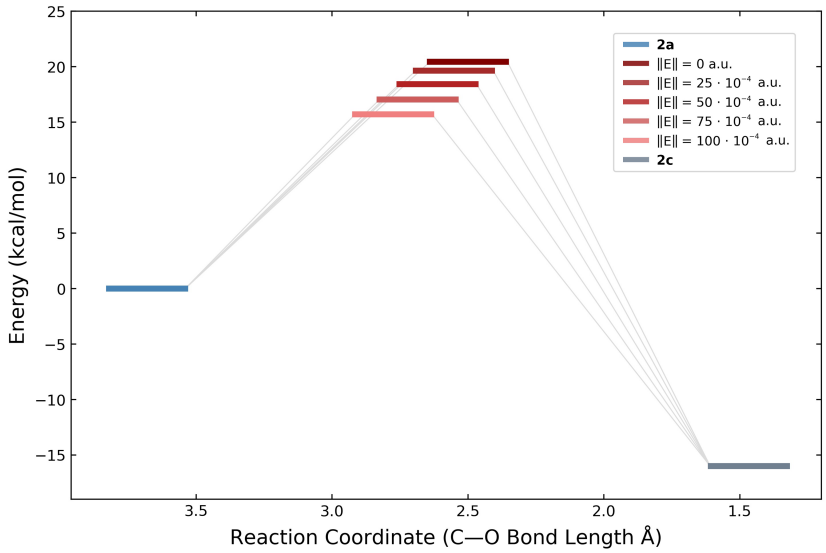

Figure 8: Reaction coordinate representation of **2**. The transition state **2b** occurs earlier and lower in energy as a result of stronger optimally oriented electric field.

Correlation between Activation Energy Reduction and Dipole Moment Magnitude. A relationship between the absolute reduction in activation energy and the magnitude of $\Delta\vec{\mu}$ emerged from the pericyclic reaction data set. For each reaction, the largest $\Delta\Delta E^{\ddagger}$ computed across atom ordering methods was plotted against $||\Delta\vec{\mu}||$ (Figure 9). The results

indicate a strong linear correlation between the dipole difference magnitude and the realized transformation barrier reduction implying reactions with large $||\Delta\vec{\mu}||$ are more susceptible to beneficial OEF applications.

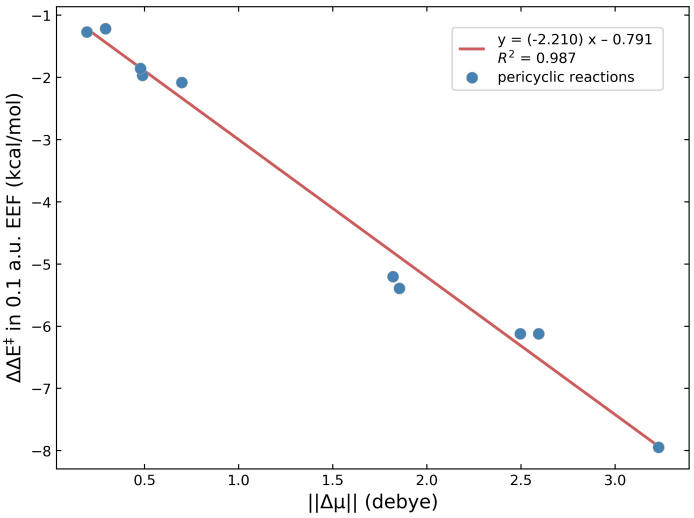

Figure 9: Relationship between $\Delta\Delta E^{\ddagger}$ due to an applied electric field and the $\|\Delta\vec{\mu}\|$ of ts_{cart} and int_{cart}. Linear regression to $y = (-2.210)\,x - 0.791$ shown in red.

Scope of A.V.E.D.A. Applications. Although A.V.E.D.A. was developed and tested on the pericyclic reactions comprising the training data set, its design facilitates broad applications. User's computations have no constraint on system size, computer resource caps, or run time limits barring those controlled by Slurm. While optimization times will depend on system size, the local A.V.E.D.A. calculations and processes remain virtually unchanged. Furthermore multiple predefined atom ordering methods, variable level of theory, detailed documentation, and fully open source software enable broad customization for computationally challenging instances. The simple initiation requirements, lack of user intervention and computational skill requirement lend A.V.E.D.A. to be a powerful tool for experimental chemists.

Conclusions

The computational workflow described herein offers a simple tool for evaluation of chemical reactions in optimally oriented electric fields using density functional theory. A.V.E.D.A. is controlled by a one-time command with user specifications, making the program highly accessible novice computational users. Results are discussed for a set of pericyclic reaction case studies, for which significant barrier reduction is predicted as a function of electric fields application along the $\Delta\vec{\mu}$ dipole difference vector. Structural changes due to the electric fields are considered in addition to the relationship between dipole moment magnitude and absolute barrier reduction. These insights bolster the promise of OEF applications to modulate chemical reactivity and improve accessibility of computational tools to support this effort.

Computational Methods and Implementation

The complete workflow for all A.V.E.D.A. processes was developed in Python 3 and Bash script intended for use on a Slurm cluster organized computer running a Linux operating system. The Gaussian 16 module is loaded and executed for all density functional theory calculations throughout the workflow.[24] Structural analysis, visualization, and presentation was facilitated by Avogadro 1.2.0, GaussView 6, UCSF Chimera, and CYLview20.[25–28]

All pericyclic data set optimizations were computed at the level of B3LYP/Def2TZVP with uncorrected energies reported. All reported structures were confirmed with normal vibrational mode analyses yielding zero imaginary frequencies for local minima and a single imaginary frequency for transition states. The complete pericyclic data set geometries—optimized at all field strengths for each successful atom ordering method—may be found on the Kennedy laboratory GitHub.[29]

Each instance of A.V.E.D.A. requires *.xyz* intermediate and transition state geometries, with corresponding atoms numbered consistently, to be in the same directory as the *start.sh* script and *Program* folder. When called, this script handles all setup and execution of the

A.V.E.D.A. workflow and thus must be provided with computation specific user arguments. First, charge and multiplicity must be entered corresponding to the overall charge and electron configuration of the given transformation. The desired level of theory is indicated with a functional and basis set argument as well as the method for atom reordering (see Results and Discussion for details). Finally, computer resources are allocated from Slurm by the desired number of processors and compute node. Note, all input parameters must be satisfied or A.V.E.D.A. will return an error and stop instantiation.

A.V.E.D.A. may be installed, edited, modified, and distributed, protected under the open source MIT License, from the Kennedy laboratory GitHub.[29]

Supporting Information Available

The following files are available free of charge.

- Supplementary figures (PDF)

Acknowledgement

The authors thank the University of Rochester for financial support of this research. D.H. acknowledges the University of Rochester Discover Grant for a research fellowship. The authors thank Prof. Ignacio Franco (University of Rochester), Prof. Pengfei Huo (University of Rochester), Prof. Andrew White (University of Rochester), and Aliza Panjwani (University of Rochester) for helpful discussions. Computations were performed on the Center for Integrated Research Computing (CIRC) BlueHive cluster at the University of Rochester; the authors are grateful for the CIRC team for their guidance.

References

(1) Shaik, S.; de Visser, S. P.; Kumar, D. External Electric Field Will Control the Selectivity of Enzymatic-Like Bond Activations. *J. Am. Chem. Soc.* **2004**, *126*, 11746–11749.

(2) Shaik, S.; Ramanan, R.; Danovich, D.; Mandal, D. Structure and reactivity/selectivity control by oriented-external electric fields. *Chem. Soc. Rev.* **2018**, *47*, 5125–5145.

(3) Shaik, S.; Danovich, D.; Joy, J.; Wang, Z.; Stuyver, T. Electric-Field Mediated Chemistry: Uncovering and Exploiting the Potential of (Oriented) Electric Fields to Exert Chemical Catalysis and Reaction Control. *J. Am. Chem. Soc.* **2020**, *142*, 12551–12562.

(4) Shaik, S.; Mandal, D.; Ramanan, R. Oriented electric fields as future smart reagents in chemistry. *Nat. Chem.* **2016**, *8*, 1091–1098.

(5) Warshel, A. Electrostatic basis of structure-function correlation in proteins. *Acc. Chem. Res.* **1981**, *14*, 284–290.

(6) Warshel, A.; Sharma, P. K.; Kato, M.; Xiang, Y.; Liu, H.; Olsson, M. H. M. Electrostatic Basis for Enzyme Catalysis. *Chem. Rev.* **2006**, *106*, 3210–3235.

(7) Kollman, P. A.; Kuhn, B.; Donini, O.; Perakyla, M.; Stanton, R.; Bakowies, D. Elucidating the Nature of Enzyme Catalysis Utilizing a New Twist on an Old Methodology: Quantum MechanicalFree Energy Calculations on Chemical Reactions in Enzymes and in Aqueous Solution. *Acc. Chem. Res.* **2001**, *34*, 72–79.

(8) Martí, S.; Andrés, J.; Moliner, V.; Silla, E.; Tuñón, I.; Bertrán, J. Preorganization and Reorganization as Related Factors in Enzyme Catalysis: The Chorismate Mutase Case. *Chem. Eur. J.* **2003**, *9*, 984–991.

(9) Szefczyk, B.; Mulholland, A. J.; Ranaghan, K. E.; Sokalski, W. A. Differential Transition-State Stabilization in Enzyme Catalysis: Quantum Chemical Analysis of

Interactions in the Chorismate Mutase Reaction and Prediction of the Optimal Catalytic Field. *J. Am. Chem. Soc.* **2004**, *126*, 16148–16159.

(10) Martí, S.; Roca, M.; Andrés, J.; Moliner, V.; Silla, E.; Tuñón, I.; Bertrán, J. Theoretical insights in enzyme catalysis. *Chem. Soc. Rev.* **2004**, *33*, 98–107.

(11) Suydam, I. T.; Snow, C. D.; Pande, V. S.; Boxer, S. G. Electric Fields at the Active Site of an Enzyme: Direct Comparison of Experiment with Theory. *Science* **2006**, *313*, 200–204.

(12) Huang, X. et al. Electric field-induced selective catalysis of single-molecule reaction. *Sci. Adv.* **2019**, *5*, eaaw3072.

(13) Wang, Z.; Danovich, D.; Ramanan, R.; Shaik, S. Oriented-External Electric Fields Create Absolute Enantioselectivity in Diels–Alder Reactions: Importance of the Molecular Dipole Moment. *J. Am. Chem. Soc.* **2018**, *140*, 13350–13359.

(14) Meir, R.; Chen, H.; Lai, W.; Shaik, S. Oriented Electric Fields Accelerate Diels–Alder Reactions and Control the endo/exo Selectivity. *ChemPhysChem* **2010**, *11*, 301–310.

(15) Aragonès, A. C.; Haworth, N. L.; Darwish, N.; Ciampi, S.; Bloomfield, N. J.; Wallace, G. G.; Diez-Perez, I.; Coote, M. L. Electrostatic catalysis of a Diels–Alder reaction. *Nature* **2016**, *531*, 88–91.

(16) Gorin, C. F.; Beh, E. S.; Bui, Q. M.; Dick, G. R.; Kanan, M. W. Interfacial Electric Field Effects on a Carbene Reaction Catalyzed by Rh Porphyrins. *J. Am. Chem. Soc.* **2013**, *135*, 11257–11265.

(17) Gorin, C. F.; Beh, E. S.; Kanan, M. W. An Electric Field–Induced Change in the Selectivity of a Metal Oxide–Catalyzed Epoxide Rearrangement. *J. Am. Chem. Soc.* **2012**, *134*, 186–189.

(18) Ciampi, S.; Darwish, N.; Aitken, H. M.; Díez-Pérez, I.; Coote, M. L. Harnessing electrostatic catalysis in single molecule, electrochemical and chemical systems: a rapidly growing experimental tool box. *Chem. Soc. Rev.* **2018**, *47*, 5146–5164.

(19) Léonard, N. G.; Dhaoui, R.; Chantarojsiri, T.; Yang, J. Y. Electric Fields in Catalysis: From Enzymes to Molecular Catalysts. *ACS Catal.* **2021**, *11*, 10923–10932.

(20) Weberg, A. B.; Murphy, R. P.; Tomson, N. C. Oriented internal electrostatic fields: an emerging design element in coordination chemistry and catalysis. *Chem. Sci.* **2022**, *13*, 5432–5446.

(21) Besalú-Sala, P.; Solà, M.; Luis, J. M.; Torrent-Sucarrat, M. Fast and Simple Evaluation of the Catalysis and Selectivity Induced by External Electric Fields. *ACS Catal.* **2021**, *11*, 14467–14479.

(22) Yoo, A. B.; Jette, M. A.; Grondona, M. SLURM: Simple Linux Utility for Resource Management. **2003**, 44–60.

(23) Schrödinger, L. The PyMOL Molecular Graphics System. 2010; `https://pymol.org/2/`.

(24) Frisch, M. J. et al. Gaussian16 Revision C.01. 2016; `https://gaussian.com`, Gaussian Inc. Wallingford CT.

(25) Hanwell, M. D.; Curtis, D. E.; Lonie, D. C.; Vandermeersch, T.; Zurek, E.; Hutchison, G. R. Avogadro. `http://avogadro.cc/`, Avogadro: an open-source molecular builder and visualization tool.

(26) Dennington, R.; Keith, T. A.; Millam, J. M. GaussView Version 6. 2019; `https://gaussian.com`, Semichem Inc. Shawnee Mission KS.

(27) Pettersen, E.; Goddard, T.; Huang, C.; Couch, G.; Greenblatt, D.; Meng, E.; Ferrin, T.

UCSF Chimera–a visualization system for exploratory research and analysis. *J Comput Chem.* **2004**, *25*, 1605–1612.

(28) Legault, C. CYLview20. 2009; `http://www.cylview.org/`.

(29) Hanaway, D.; Kennedy, C. R. A.V.E.D.A. `https://github.com/kennedy-lab-ur/A.V.E.D.A.`

TOC Graphic